limit afforded by allowing the ferrite core in the N_1 and N_2 windings to saturate is temperature dependent. If the pick-up transformer is left in an open-circuit condition for a long period of time the performance approaches the lower limit line (ferrite hot), while when the ferrite is cold the upper voltage limit line is operable and in practice is able to protect the Schottky rectifiers from over-voltage conditions. The change in current over the working range of the device is attributable to the finite Q of the windings. The leakage inductance can be inferred (direct measurement is impossible) by comparing the AC voltage on the N_2 winding with the output DC voltage. Over the range 0–15.75 V with the ferrite hot or cold this relationship has been measured to be

$$V_{DC} = \frac{N_1}{N_2}\frac{2\sqrt{2}}{\pi}V_{N_2} - 0.004I_{DC} - 0.6$$

with a maximum error < 100 mV.

Here, the first term is the expected rectified voltage, the second term is caused by the commutation overlap of the diodes (corresponding to an overlap angle of 30°) and the third term is the voltage drop in the Schottky diodes. Thus, the commutation reactance is 4 mΩ so that $(l_2' + l_1)$ is ~78 nH which is ~14% of $(L_m + l_2')$. This leakage reactance includes the inductance of the rectifier busbars and is a very pleasing figure for a single turn transformer.

Conclusions: A new pick-up transformer for ICPT applications has been described. The device allows very high voltage or very high current outputs to be produced and controlled directly from an ICPT system using low-cost semiconductor switches with modest ratings. In a practical example, a single turn pick-up transformer and rectifier produces an output of 270 A with a current regulation of 3% as the output voltage varies from 0–15.75 V DC.

9 July 2002
Electronics Letters Online No: 20020874
DOI: 10.1049/el:20020874

J.T. Boys, G.A. Covic and G.A.J. Elliott (*Department of Electrical and Electronic Engineering, School of Engineering, The University of Auckland, Private Bag 92019, Auckland, New Zealand*)

E-mail: mailto:j.boys@auckland.ac.nz

References

1 LAOUAMER, R., BRUNELLO, M., FERRIEUX, J.P., NORMAND, O., and BUCHHEIT, N.: 'A multi-resonant converter for non-contact charging with electromagnetic coupling'. 23rd Int. Conf. on Industrial Electronics, Control and Instrumentation, IECON97, New Orleans, USA, 1997, Vol. 2, pp. 792–797

2 SAKAMOTO, H., HARADA, K., WASHIMIYA, S., TAKEHARA, K., MATSUO, Y., and NAKAO, F.: 'Large air-gap coupler for inductive charger [for electric vehicles]', *IEEE Trans. Magn.*, 1999, **35**, (5), pp. 3526–3528

3 PEDDER, D.A.G., and BROWN, A.D.: 'A contactless electrical energy transmission system', *IEEE Trans. on Ind. Electron.*, 1999, **46**, (1), pp. 23–30

4 ABE, H., SAKAMOTO, H., and HARADA, K.: 'A noncontact charger using a resonant converter with parallel capacitor of the secondary coil', *IEEE Trans. Ind. Appl.*, 2000, **36**, (2), pp. 444–451

5 BOYS, J.T., COVIC, G.A., and GREEN, A.W.: 'Stability and control of inductively coupled power transfer systems', *IEE Proc., Electr. Power Appl.*, 2000, **147**, (1), pp. 37–43

CPM for indoor wireless channel

G.P. Chapelle

This research investigates the degradation in performance when a continuous phase modulated system is operated over an indoor wireless channel that is characterised by slow frequency-selective Rician fading and multiple cochannel interferers.

Introduction: Continuous phase modulation (CPM) is ideal where inexpensive nonlinear amplifiers are desired and band-limiting is present, due to its constant envelope and narrow spectrum.

The Viterbi algorithm for demodulation of CPM was investigated by several authors [1] for two-ray multipath fading [2] and with interference [3], where it was discovered that binary modulation performed better than quaternary schemes. The research described in this Letter extends the two-ray fading case [2] to an arbitrary number of multipaths, with potentially different powers, and expands [3] to multiple interferers the frequency deviations of which may be distinct from the desired signal.

Modulation and channel models: CPM has symbol energy E, symbol period T, frequency ω_c, and the transmitted form $s(t, \vec{\alpha}) = \sqrt{(2E/T)}\cos[\omega_c t + \phi(t, \vec{\alpha})]$. The phase function $\phi(t, \vec{\alpha})$ contains the sequence, $\vec{\alpha}$, of M-ary data, $\alpha_i \in \{\pm 1, \pm 3, \ldots, \pm(M-1)\}$, with M a power of two. The phase function is a normalised integral of the frequency pulse describing how the underlying phase changes, $2\pi h\alpha_i$, evolve with time, and the deviation ratio h is a non-negative real-valued constant, restricted to obey the relationship $h = 2r/m$, for r and m integers, resulting in only m CPM states.

Utilising the Rician multipath fading model [4] for indoor channels having complex lowpass equivalent channel response for L paths, given by

$$h(t) = Ae^{j\mu}\delta(t-\zeta) + \sum_{l=1}^{L}\beta_l e^{j\gamma_l}\delta(t-\tau_l) \qquad (1)$$

with non-varying gain A of the specular component having range [0, 1], and non-varying phase μ and delay ζ due to signal transmission delay. A Rayleigh amplitude gain, β_l, with $E(\beta_l^2) = 2\rho_l$, and the random phase, γ_l, is uniformly distributed $U[0, 2\pi]$. The random time delay, τ_l, is assumed uniformly distributed over a symbol period $U[0, T]$. All of the gains, delays, and phases of different paths are assumed to be statistically independent, and remain constant during short data transmissions. Using the ratio of the specular component power to the fading power, expressed by a lowpass equivalent channel model as $H_l = A^2/(2\rho_l)$, measurements [4] show H_l ranges from 6 to 12 dB for the indoor channel.

Maximum likelihood sequence detection: For CPM the MLSE is a maximised log likelihood function and is equal to a correlation over one symbol period $[nT, (n+1)T]$ of possible CPM signals $s_{ij}(t, \vec{\tilde{\alpha}}) = \sqrt{(2P)}\cos\{\omega_c t + \theta_{i(n-1)} + \theta(t, \tilde{\alpha}_{jn})\}$ with the received CPM signal $r(t)$ plus noise, with $nT \le t \le (n+1)T$, and $i = (1, 2, 3, \ldots m)$ and $j = (1, 2, 3, \ldots M)$. In s_{ij}, $\vec{\tilde{\alpha}}$ is the estimated data sequence, $\theta_{i(n-1)}$ is the correlative state, and $\theta(t, \tilde{\alpha}_{jn})$ is the phase state at time n. For the M possible values of the estimated symbols and m possible phase states, there are $m \cdot M$ different correlation values computed in each signal interval, with each value used to increment the previous interval metric.

Determining the probability of error: With an MLSE the lth received signal path is

$$r_l(t) = s(t-\tau_l, \vec{\alpha}) + \sum_{k=1}^{K} I(t-\tau_k-\tau_{kl}, \theta_k, \vec{\alpha}_k) + n(t) \qquad (2)$$

where $s(t-\tau_l, \vec{\alpha})$ is the desired signal, $I(t-\tau_k-\tau_{kl}, \theta_k, \vec{\alpha}_k)$ is the kth interfering signal, and $n(t)$ is conditionally Gaussian noise, as shown in [5]. The τ_k are random variables uniformly distributed $U[0, T]$ over one symbol, and θ_k are r.v. uniformly distributed in phase $U[0, 2\pi]$, accounting for the random transmission delay for each of the K interferers. Likewise, the τ_l and τ_{kl}, are r.v. uniformly distributed $U[0, T]$ accounting for the lth multipath delay of the desired signal and kth interfering signal, respectively. All of the τ_k, τ_l, τ_{kl}, and θ_k are independent of each other. The interfering signals are also CPM, but may use a different deviation ratio value h_k from the desired signal, and are still subject to the Rician channel.

A state description can be used to denote the estimated state at time j, from the Viterbi algorithm, against the estimated symbols $\{\tilde{\alpha}_n\}$ as $\tilde{s}_j = \{\tilde{\theta}_{j-1}, \theta(t, \tilde{\alpha}_j)\}$. Now if the estimated path through the trellis diverges from the correct path at time j and merges with the correct path at time $j+m$, then $\tilde{s}_j = s_j$ and $\tilde{s}_{j+m} = s_{j+m}$, but $\tilde{s}_n \neq s_n$, for $j < n < j+m$, for an error event of length m. For such an error event, $\tilde{\alpha}_j \neq \alpha_j$ and $\tilde{\alpha}_{j+m-1} \neq \alpha_{j+m-1}$ and $\tilde{\alpha}_n = \alpha_n$ for $n \in [j+1, j+m-1]$,

$m \geq 2$. The probability of error for a particular error event beginning at time j is calculated from a procedure [6], requiring three sub-events in order for the error event vector to occur. These three events are: (i) the diverging branches begin from a common branch, (ii) all diverging branches must be from allowable data sequences, and (iii) the sum of the branch metrics for the incorrect path must exceed those for the correct path. All three events occur in this model.

The details of the calculation [5] result in the upper bound on the error probability averaged over all of the random variables for the L multipaths and K interfering users. This is written

$$\Pr[E] \leq \sum_{\vec{\alpha}_m} \sum_{\vec{\tilde{\alpha}}_m \neq \vec{\alpha}_m} w(\vec{\alpha}_m, \vec{\tilde{\alpha}}_m) \prod_{i=0}^{m-1} \frac{M - |\hat{e}_i|}{M} \times \left[\frac{1}{2^{K(m+1)}} \sum_{k=1}^{2^{(m+1)}} \frac{1}{T^K} \frac{1}{T^L} \frac{1}{T^{KL}} \frac{1}{(2\pi)^K} \int_0^T \int_0^T \int_0^T \int_0^{2\pi} Q\left(\frac{d_s^2(\vec{\alpha}_m - \vec{\tilde{\alpha}}_m) + x_l(\vec{\alpha}_m, \vec{\tilde{\alpha}}_m, \vec{\alpha}_k, \theta_K, \tau_K)}{\sqrt{\sigma^2_{N_m}(\vec{\alpha}_m, \vec{\tilde{\alpha}}_m, \vec{\tilde{\alpha}}_k, \theta_K, \tau_K, \tau_L, \tau_{KL})}} \right) d\theta_K \, d\tau_K \, d\tau_{KL} \, d\tau_L \right] \tag{3}$$

The k summation is multidimensional, with the number of dimensions equal to the number of interferers K. The integrations over τ_K and θ_K are each K-dimensional, the integration over τ_{KL} is a $K \cdot L$-dimensional integration and the integration over τ_L is an L-dimensional integration. The distance d_s^2 between the signal and estimate, and the interference terms x_l are calculated in [5]. The noise variance, $\sigma^2_{N_m}$, is worked out in detail [5], and is due to both the AWGN and the diffuse multipaths of the $K+1$ users. The AWGN component of this variance is given by

$$\sigma^2_{awgn} = 2\eta_0 \sum_{i=0}^{m-1} \int_{iT}^{(i+1)T} [s(t, \vec{\alpha}) - s(t, \vec{\tilde{\alpha}})]^2 dt = 2\eta_0 d^2_{s_m} \tag{4}$$

The desired signal contribution to the conditional variance is calculated in [5] and is equal to

$$\sigma^2_{multi_m} = 4P^2 \sum_{l=1}^{L} \rho_l (C_l^2 + S_l^2) \tag{5}$$

and the contribution of the K interferers to the conditional variance, conditioned on τ_{kl} and $\vec{\alpha}_k$ is [5]

$$\sigma^2_{int_m} = \sum_{k=1}^{K} P_k \sum_{l=1}^{L} \rho_{kl} (C_{kl}^2 + S_{kl}^2) \tag{6}$$

where C_l and S_l are equal to

$$C_l = \sum_{i=0}^{m-1} \int_{iT}^{(i+1)T} (\cos\{\phi(t - \tau_l, \vec{\alpha}) - \phi(t, \vec{\alpha})\} - \cos\{\phi(t - \tau_l, \vec{\alpha}) - \phi(t, \vec{\tilde{\alpha}})\}) \, dt \tag{7}$$

and

$$S_l = \sum_{i=0}^{m-1} \int_{iT}^{(i+1)T} (\sin\{\phi(t - \tau_l, \vec{\alpha}) - \phi(t, \vec{\alpha})\} - \sin\{\phi(t - \tau_l, \vec{\alpha}) - \phi(t, \vec{\tilde{\alpha}})\}) \, dt \tag{8}$$

The expressions for C_{kl} and S_{kl} are similar, but with τ_{kl} and $\vec{\alpha}_k$ substituted for τ_l and $\vec{\alpha}$ in the expressions for C_l and S_l. Finally, P is the desired signal power, P_k is the kth interfering signal power, and ρ_l and ρ_{kl} are from the Rayleigh components of the desired and interfering signals, respectively. The total conditional variance is then given by the sum of (4), (5), and (6) as $\sigma^2_{N_m} = \sigma^2_{awgn} + \sigma^2_{mult_m} + \sigma^2_{int_m}$.

Numerical results: Monte Carlo integration methods are used to increase the computational speed of (3). The error performance for three interferers using 1REC, all with identical powers, is found in [5], where the best performance obtained was by $h = 2/3$ and $3/4$, because these are near the optimum deviation ratio of $h = 0.715$ for AWGN.

When multipath fading is present, (3) is averaged over the random multipaths and delays. The multipaths can have a constant power profile or an exponentially decaying profile. The constant power profile results are shown in [5]. The exponentially decaying multipath profile rate is selected so the second multipath is one half the power of the first, and the third is one fourth the power of the first. The channel ratio value H_l is then equal to the largest multipath received, or equivalently by the first multipath.

The case of a decaying four multipath power profile is shown in Fig. 1. In deep fading with $H = 6$ dB, the error performance shows a characteristic error floor. At small SNR, the error performance is nearly equivalent between $h = 2/3$ and $4/5$. In mild fading with $H = 12$ dB, all frequency deviations perform well and the error floor is below 10^{-8} for the best index of $h = 2/3$.

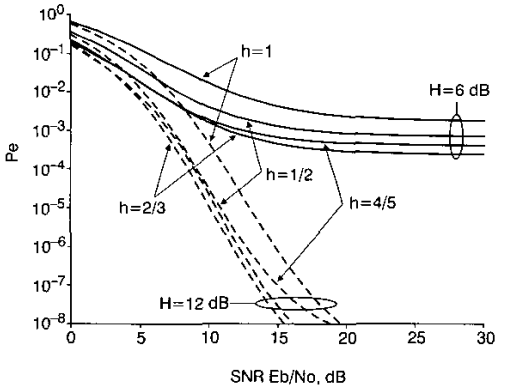

Fig. 1 *Performance with three decaying power multipaths*
Binary, $L = 3$, $K = 0$, 1REC, decay profile

The performance for CPM can be compared with Gaussian MSK by using the results in [7] for the symbol error probability of GMSK with differential detection in Rician fading. The GMSK performance is calculated for a premodulation filter parameter of $BT = 0.5$, and is plotted in Fig. 2 for the Rician factors used in [7], along with 1REC CPM for three constant power multipaths. For small Rician factors, the performance of 1REC is slightly poorer than the GMSK, due particularly to a cascading of errors in the MLSE detector, while for larger Rician factors 1REC performs significantly better than GMSK due to the modulation memory. The GMSK system is more spectrally efficient, but increased spectral efficiency is possible by using CPM with improved spectral efficiency like 1RC and 2RC, while still maintaining the excellent error performance.

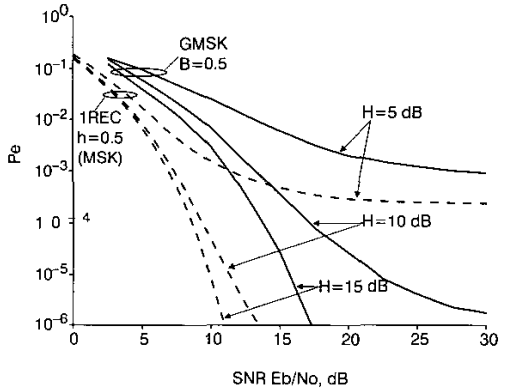

Fig. 2 *CPM against GMSK in single multipath Rician fading*

Conclusions: The MLSE was analysed for CPM operating on the indoor wireless channel, characterised by cochannel interference and Rician multipath fading. The degrading effects of the interference and fading for four deviation ratio values of CPM with an MLSE were examined and the modulation index of $h = 2/3$ performed the best. A comparison with currently used GSM receivers was found to achieve better error performance for moderate fading and larger SNRs. The dominant effect on performance was found to be the multipath fading. Further study is possible with (3) of interferers with different

modulation indices and powers, along with a family of fading power profiles possible, but limited space prevents discussing these rich areas.

22 July 2002
Electronics Letters Online No: 20020884
DOI: 10.1049/el:20020884

G.P. Chapelle (*Nokia Mobile Phones, San Diego Product Creation Center, 12278 Scripps Summit Drive, San Diego, California 92131, USA*)

References

1 ANDERSON, J., AULIN, T., and SUNDBERG, C.-E.: 'Digital phase modulation' (Plenum Press, 1986)
2 SVENSSON, N.A.B.: 'On optimum and suboptimum coherent detection of continuous phase modulation on a two-ray multipath fading channel', *IEEE Trans. Commun.*, 1987, **35**, (10), pp. 1041–1049
3 SVENSSON, N.A.B.: 'Error probability analysis for continuous phase modulation with Viterbi detection on a Gaussian channel with multiple signal interference', *IEEE Trans. Commun.*, 1989, **37**, (3), pp. 230–237
4 HASHEMI, H.: 'The indoor radio propagation channel', *Proc. IEEE*, 1993, **81**, (7), pp. 943–968
5 CHAPELLE, G.: 'Continuous phase modulation for the indoor wireless channel'. Ph.D. Dissertation, Department of Electrical and Computer Engineering, University of California, San Diego, CA, USA, 1998
6 FORNEY, G.D.: 'Maximum-likelihood sequence estimation of digital sequences in the presence of intersymbol interference', *IEEE Trans. Inf. Theory*, 1972, **18**, pp. 363–378
7 SMITH, W.S., and WITTKE, P.H.: 'Differential detection of GMSK in Rician fading', *IEEE Trans. Commun.*, 1994, **42**, (2/3/4), pp. 216–220

Filter-shaped LMS algorithm-based predictive power control

H.S.H. Gombachika, B.G. Evans and R. Tafazolli

A predictive closed-loop power control scheme based on a filter-shaped least-mean-square (FS-LMS) algorithm, which takes into account knowledge of the fading process time-evolution, is proposed. It is demonstrated through simulation, that an FS-LMS-based closed-loop power control scheme performs better than the standard LMS algorithm.

Introduction: In the satellite environment, fast closed-loop power control is considered less effective because of long propagation delays. Nevertheless, a slow closed-loop power control scheme will be used in satellite UMTS (S-UMTS), where transmitted power is updated once every frame (10 ms) instead of once every time-slot.

To mitigate the effects of excessive delays in satellite networks, predictive schemes can be used, through which the dynamics of the channel fading process are modelled as an autoregressive (AR) process. The AR process is then realised as an 'all-pole' transversal adaptive filter, the coefficients of which are dynamically adjusted using recursive algorithms. For slow closed-loop power control, a recursive algorithm based on the least-mean-square (LMS) algorithm is sufficient [1].

The LMS algorithm was developed based on an assumption that the coefficients of the adaptive filter evolve with time in a completely unpredictable manner, i.e. the the evolutionary process is white. However, for the land mobile satellite system (LMSS) channel slow-fading process, the statistical properties are well established and indicate that the slow-fading process is band-limited. This knowledge can be incorporated in the adaptive algorithm to improve on the performance offered by the standard LMS algorithm [2].

In this Letter therefore, we use the knowledge on the way the channel slow-fading process evolves with time to improve the performance of predictive closed-loop power control schemes. We propose a filter-shaped LMS (FS-LMS) algorithm that limits the bandwidth of the evolving process of the adaptive filter coefficients. We demonstrate, through simulation, that the FS-LMS-based closed-loop power control scheme performs better than the standard LMS algorithm. Furthermore, we show that the FS-LMS algorithm offers an additional degree-of-freedom for enhancing the performance of closed-loop power control schemes.

Filter-shaped LMS algorithm: A block diagram of a closed-loop power control scheme based on the FS-LMS algorithm is shown in Fig. 1. Let $x(n)$ denote a baseband sample value of the channel-state at time (n), and $\hat{x}(n)$ the predicted value of $x(n)$ defined as

$$\hat{x}(n) = \sum_{i=1}^{p} \hat{w}_i(n) x(n-i) \tag{1}$$

where p is the order of the predictor, and the weights $\hat{w}_i(n)$ are predictor coefficients. The values of the predictor coefficients are set to minimise a cost function $J(w) = E[(x(n) - \hat{x}(n))^2]$, where $E[\cdot]$ denotes statistical expectation.

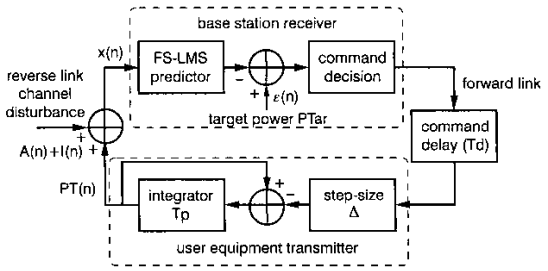

Fig. 1 *FS-LMS based closed-loop power control model*

For a nonstationary channel such as the LMSS link, values of the predictor coefficients are dynamically determined by recursive methods. In slow closed-loop power control schemes, the least-mean-square (LMS) algorithm can sufficiently be used to determined the values of the predictor coefficients.

The standard LMS algorithm was developed on an assumption that the coefficients of the channel model evolve with time in a completely unpredictable manner. However, for the satellite link, the statistical properties of the channel are well established, and show that the slow fading process due to shadowing is band-limited, which is modelled as as a first-order filter [3] as

$$w_i(n+1) = \alpha w_i(n) + \eta(n) \tag{2}$$

where $w_i(n)$ is the ith coefficient of the fading process model, and $\eta(n)$ is white Gaussian process. α is related to the user-equipment speed, channel correlation-distance and location variability (σ_L). We use this knowledge to modify the LMS-based power control schemes to improve the performance offered by closed-loop power control schemes. The LMS is therefore modified by including a rational shaping-filter to band-limit the process noise, resulting in the FS-LMS algorithm described as follows.

The algorithm is first initialised by setting $\hat{w}_o = 0$, where 0 is a null vector. During each power control period (T_p), the tap weights are updated as

$$\xi(n) = x(n) - \hat{w}_n^T \mathrm{x}_n$$
$$\hat{w}_{n+1} = (1+\alpha)\hat{w}_n - \alpha\hat{w}_{n-1} + \mu \mathrm{x}_n \xi^*(n) \tag{3}$$

where $\mathrm{x}_n^T = [x(n-1), \cdots, x(n-p+1)]$ is a vector containing past input data, μ is an adaption step-size, and α: $\{0 < \alpha < 1\}$ is a scalar determining the location of the pole of the rational shaping-filter. When $\alpha = 0$, we get the standard LMS algorithm.

Simulation results: The objective of the link-level simulation analysis was to investigate the performance of the proposed predictive closed-loop power control scheme based on the FS-LMS algorithm with the standard LMS algorithm as a reference. The measure of performance was the standard deviation of the power control error (σ_ε). We assumed that the adaptive algorithms attempted to track the slow fading which follows a lognormal distribution characterised by variation mean (μ_L) and location variability (σ_L). Parameters assumed in this study were: power control period, $T_p = 10$ ms; predictor order, $p = 10$; adaptation step-size, $\mu = 2 \times 10^{-4}$; power control step-size, $\Delta = 1.0$ dB; carrier frequency, $F_c = 2$ GHz.